Arch. Mech., **58**, 1, pp. 125–154, Warszawa 2006

Robust identification of an augmented Gurson Model for elasto-plastic porous media

Z. NOWAK[1)], A. STACHURSKI[2)]

[1)] *Institute of Fundamental Technological Research*
Polish Academy of Sciences
Świętokrzyska 21, PL 00-049 Warsaw, Poland

[2)] *Institute of Control and Computation Engineering*
Warsaw University of Technology
Nowowiejska 15/19, 00-665 Warsaw, Poland

In the paper we investigate the robust identification approach to identify the material parameters in the augmented Gurson model for the elasto-plastic porous media. We consider the robust loss function given by Huber [9], Beaton and Tuckey [38] and the loss function based on the l_1–norm. The resulting minimization problem is solved by means of our own implementation of the Boender *et al.* global minimization method. Our aim is to compare the results with our earlier standard least squares estimates. In the paper, the effects of nucleation and growth of voids in the plastic porous media are investigated. Three different forms of the model are considered: the augmented Gurson model (total porosity model) with variable nucleation and growth material function, the same model with constant growth material function and the separated porosity model. The identification of the material functions parameters is based on Fischer's experimental data set for axisymmetric tension of steel specimens.

Key words: Gurson model, elasto-plastic porous media, robust identification, Huber loss function, Beaton and Tuckey loss function, l_1–norm loss function.

1. Introduction

The aim of the paper is to find the best model describing the nucleation and growth of voids in porous plastic body. The second purpose is to study the influence of large deviations (data inaccuracy). We investigate the robust identification approach to identify the material parameters in the augmented Gurson model for the elasto-plastic porous media. The model describes processes of nucleation and growth of voids in the porous body subjected to inelastic deformation.

The formation of microvoids in commercial grade materials is attributed to the presence of inhomogeneities. The microvoids appear either as cracks in the particles or as failure of the particle-matrix interfacial bonding. The actual microvoid morphology depends upon the interrelation of various microstructural parameters as well as the local deformation state.

There have been many studies directed toward better understanding of void evolution and developing constitutive relations for inelastic porous solids. The model by GOLOGANU *et al.* [10], SØVIK and THAULOW [39], PARDOEN and DELANNAY [32], PARDOEN, DOGHRI and DELANNAY [33] and PARDOEN and HUTCHINSON [34], accounts for void shape effects and distribution of voids, respectively. In addition, some other effects, such as the strain mode effect in a matrix (e.g. KOPLIK and NEEDLEMAN [13], Tvergaard [41], LEBLOND *et al.* [14] and LI *et al.* [15]) on the void growth, have been studied. All the analyses have shown clearly that, besides the stress triaxiality and equivalent plastic strain, there are other effects influencing the growth of voids.

The volume fraction of microvoids ξ as a function of equivalent plastic strain $\bar{\epsilon}_p$ given by FISHER [7] and FISHER and GURLAND [8] is plotted in Fig. 1. It should be stressed that Fisher's data are complete in that sense that they deliver not only the total porosity but also the nucleation part of porosity. In the first part of our calculations we have not exploited that information. Also the results presented in our two earlier papers (NOWAK and STACHURSKI [29]) have used the total measure of porosity neglecting the rest of the experimental information. This is somehow justified because the majority of the experimental results available in the literature contains only measurements of the total porosity (cf. NEEDLEMAN and RICE [27], SAJE *et al.* [2]). Our identification problem arises in modelling of the processes of nucleation and growth of voids in the elastic-plastic media. In the third NOWAK and STACHURSKI'S [30] paper we have also considered the model with separated porosities.

In all the above mentioned studies the least squares approach (i.e. the mean squares loss function) was used. In the current work we have decided to investigate the impact of the use of other deviation measures such as the Huber loss function (allowing to omit large deviations) and the l_1 loss function.

We consider the uniaxial test in the room temperature. At the neck there exists a complex state of stress and maximum deformations. Identification is carried out on the basis of FISHER's data [7] measured on the steel cylindrical specimens subjected to the uniaxial tension. We assumed that the effects of nucleation and growth of microvoids were summing up and we combined in one model, two models formulated separately for each of those two effects. Usually in literature, the material function g appearing in the model part responsible for the growth of microvoids is taken to be constant and equal to 1 (no interaction of existing or nucleated new microvoids on the growth process is included). In our work we have assumed various shapes of g. Among others we have also studied the case with a constant although unknown g function.

For the "best model" selection we have applied the Akaike and FPE tests (used to compare to the nested models) and Vuong's test to discriminate between the rival nonnested models.

2. Formulation of the identification problem

The identification problem is stated as the problem of finding values of the material function parameters ensuring minimal value of the mean square functional calculated as the value of the appropriate loss function f depending on the unknown parameters $\mathbf{x}$ and calculated with the aid of differences between the observed output values Y_i and the corresponding calculated output values $\tilde{Y}_i$ ($\tilde{Y}_i = F(\bar{\epsilon}_{p_i}, \mathbf{x})$). Here F represents the assumed model. It connects the input independent variable values, $\bar{\epsilon}_{p_i}$, with the output values, ξ_i, and accordingly $\mathbf{x}$ denotes the unknown parameters. Thus our problem is

$$\min_{\mathbf{x}\in V} f(\mathbf{x}), \tag{2.1}$$

where $V \subset R^n$ denotes the set of admissible parameters values (n is the number of the unknown parameters to be identified). We have used in our studies various forms of the loss functions specified in the subsection below.

2.1. Different forms of loss functions

The first loss function considered by us is a standard mean squares function.

Quadratic loss function

$$\min_{\mathbf{x}\in V} f(\mathbf{x}) = F_1(\mathbf{x}) = \sum_{i=1}^{M} r_i^2(\mathbf{x}), \tag{2.2}$$

where

$$r_i(\mathbf{x}) = Y_i - F(\bar{\epsilon}_i^{\mathrm{p}}, \mathbf{x}), \tag{2.3}$$

$V \subset R^n$ is the set of admissible parameters values, n is the number of the unknown parameters to be identified and M is the number of observations (measured input and the corresponding output values). $F(\bar{\epsilon}_i^{\mathrm{p}}, \mathbf{x})$ – the calculated output of the model, while Y_i is the measured output value (porosity) at the given point $\bar{\epsilon}_i^{\mathrm{p}}$. Here in the least squares formulation the objective function $\vartheta_1(t) = t^2$.

The next three loss functions allow to weaken either the influence of large deviations or their rejection. They assume different forms of the objective and loss functions.

Huber loss function [9] (see also, for example, [38] p. 650)

$$F_2(\mathbf{x}) = \sum_{i=1}^{M} \vartheta_2\left(\frac{r_i(\mathbf{x})}{\chi}\right), \tag{2.4}$$

where

$$\vartheta_2(t) = \begin{cases} t^2, & |t| \le A, \\ 2A|t| - A^2, & |t| \ge A \end{cases} \tag{2.5}$$

and χ is some measure of dispersion approximated by

$$\chi^a \approx \frac{1}{M} \sum_{i=1}^{M} |r_i(\Theta^a)|,$$

where Θ^a is an approximation to the estimate of $\mathbf{x}$.

Huber function (2.4) permits the reduction of the influence of extreme outliers creating deviations larger than a given threshold. In the least squares identification all observations were treated equally, they have the same weights.

Beaton and Tuckey robust loss function [38] p. 650 $F_3(\mathbf{x})$ is the same as the Huber loss function (2.4) but with $\vartheta(t)$ defined differently

$$\vartheta_3(t) = \begin{cases} \dfrac{1}{3}A^2 \left[1 - \left[1 - (t/A)^2\right]^3\right], & |t| \le A, \\ \dfrac{1}{3}A^2, & |t| \ge A. \end{cases} \tag{2.6}$$

l_1 **norm loss function**

$$F_4(\mathbf{x}) = \sum_{i=1}^{M} |r_i(\mathbf{x})|. \tag{2.7}$$

In this case the objective function ϑ has got the following form

$$\vartheta_4(t) = |t|. \tag{2.8}$$

The l_1–norm minimization decreases, similarly as in other robust loss functions, the influence of large deviations compared to the least squares approach. The influence function ($\phi = \vartheta_4'$) values are equal to -1 if t is negative and to 1 if t is positive and it is undefined for $t = 0$. Hence it satisfies the requirement on the robust influence function that it should be bounded as the residual observation t is tending to infinity.

2.2. Formulation of the identification problem in the case of total porosity

We focus on the problem of plastic flow and fracture of dissipative solids in which the intrinsic micro-damage effects are observed. Our aim is to find

the material parameters appearing in the material functions at the evolution equation for the porosity, ξ describing the intrinsic microdamage effects.

$$\begin{aligned}\dot{\xi} &= \dot{\xi}^n + \dot{\xi}^g \\ &= h(\bar{\epsilon}_p, \mathbf{x})\frac{1}{1-\xi}\mathrm{tr}(\boldsymbol{\sigma}\mathbf{D}^p) + g(\bar{\epsilon}_p, \mathbf{x})(1-\xi)\mathrm{tr}(\mathbf{D}^p),\end{aligned} \tag{2.9}$$

where $h(\bar{\epsilon}_p, \mathbf{x})$ and $g(\bar{\epsilon}_p, \mathbf{x})$ are the material functions, $\bar{\epsilon}_p$ is the equivalent plastic strain, $\mathbf{D}^p$ denotes the plastic rate of the deformation tensor. The details of the damage model are to be found in Sec. 3.

The identification problem is stated as the problem of finding values of the material function parameters ensuring minimal value of one of the loss functions stated in the previous section. Thus our problem is

$$\min_{x\in V} F_i(\mathbf{x}) = \sum_{j=0}^{M} \vartheta_i(r_j(\mathbf{x})), \quad i = 1, \ldots, 4, \tag{2.10}$$

where $V \subset R^n$ denotes the set of admissible parameter values (n is the number of the unknown parameters to be identified). Vector $\mathbf{x}$ denotes the unknown parameters. The $r_j(\mathbf{x}) = Y_j - \tilde{Y}_j$ is the difference between the observed output values Y_j and the corresponding calculated output values $\tilde{Y}_j$ ($\tilde{Y}_j = F(\bar{\epsilon}_{p_j}, \mathbf{x})$). Here F represents the assumed model. It connects the input independent variable values, $\bar{\epsilon}_{p_j}$, with the output values, ξ. Substitution of the formula $\tilde{Y}_j = F(\bar{\epsilon}_{p_j}, \mathbf{x})$ into (4.8) yields

$$\min_{\mathbf{x}\in V} \sum_{j=1}^{M} \vartheta_i\left(Y_j - F(\bar{\epsilon}_{p_j}, \mathbf{x})\right), \quad i = 1, \ldots, 4. \tag{2.11}$$

The second term in formula (4.11) represents the calculated output values $\tilde{Y}_j$, and again M is the number of observations (measured input and the corresponding output values). In fact we have solved four different minimization problems. Each problem corresponds to a different loss function $\vartheta_i(t)$, $i = 1, 2, 3, 4$.

In our primal problem the calculated output is obtained as a result of the integration of an ordinary differential equation, where on the left-hand side its derivative with respect to the input $\bar{\epsilon}_p$ appears. The right-hand side of the differential equation depends on the input and output variables and on unknown parameters. The unknown parameters appear exclusively in the so-called material functions being a part of the right-hand side of the differential equation. See for details Secs 3. and 4.

The parameters should belong to the set V of feasible values of parameters, defined in Sec. 8. In this part we have not made any use of the data on the growth or nucleation volume fractions, although they are available in the Fisher's data set.

2.3. Formulation of the identification problem in the case of separated nucleation and growth porosity

The Fisher's data set contains not only the values of the total porosity but also the corresponding separated nucleation and the growth porosity. Therefore we have decided to change accordingly the identified model to the form of two separate evolution equations – the first one describing the nucleation of new voids and the second one describing growth of the already existing voids. Those differential evolution equations are mutually connected by introduction of the total porosity into their right-hand sides as follows:

$$\begin{aligned} \dot{\xi}^n &= h(\bar{\epsilon}_p)\frac{1}{1-\xi^n-\xi^g}\mathrm{tr}(\boldsymbol{\sigma}\mathbf{D}^p), \\ \dot{\xi}^g &= g(\bar{\epsilon}_p)(1-\xi^n-\xi^g)\mathrm{tr}(\mathbf{D}^p). \end{aligned} \tag{2.12}$$

This means that we keep the additivity assumption saying that total porosity ξ is the sum of the nucleation and growth effects, i.e. $\xi = \xi^n + \xi^g$. The model represented by Eqs. (2.12) is not mathematically equivalent to the model (2.9). Anyhow, we believe it is justified on the basis of the existing models describing separately the phenomena of nucleation of new voids and growth of the existing voids. The only difference is the replacement of the partial ξ on the right-hand sides by the total porosity.

The above presented change in the model formulation is reflected in the loss functions (4.11). Here we sum up the values of the loss function calculated separately for the nucleation and growth parts.

$$\min_{\mathbf{x}\in V}\left[\sum_{j=1}^{M}\vartheta_i\left(\bar{\xi}_j^n-\xi^n(\bar{\epsilon}_{p_j},\mathbf{x})\right)+\sum_{j=1}^{M}\vartheta_i\left(\bar{\xi}_j^g-\xi^g(\bar{\epsilon}_{p_j},\mathbf{x})\right)\right],\quad i=1,\ldots,4. \tag{2.13}$$

Here, $\bar{\xi}^n$ and $\xi^n(\bar{\epsilon}_{p_j},\mathbf{x})$ denote the experimental and calculated (for given parameters $\mathbf{x}$) values of the nucleation of new voids and $\bar{\xi}^g$ and $\xi^g(\bar{\epsilon}_{p_j},\mathbf{x})$ denote the experimental and calculated values of the growth of existing voids, respectively. Calculated values $\xi^n(\bar{\epsilon}_{p_j},\mathbf{x})$ and $\xi^g(\bar{\epsilon}_{p_j},\mathbf{x})$ are obtained by the numerical integration of the differential evolution equations (2.12).

We have used the same sets of material functions as in the total formulation.

3. Porosity model

The microvoids appear either as cracks in the particles or as failure of the particle-matrix interfacial bonding. The actual microvoid morphology depends upon the interrelation of various microstructural parameters as well as the local deformation state. It is postulated that the evolution equation for porosity

parameter has the form (2.9) (cf. NEEDLEMAN and RICE [27], PERZYNA [36] or PERZYNA and NOWAK [37]). The first term in the evolution equation (2.9) for the porosity parameter ξ describes cracking of hard, brittle particles or debonding of second-phase particles from the matrix as the plastic work progressively increases. In Fisher's data, in steel of type B (with 0.17%C) the nucleation of voids is generated mainly by debonding of the cementite particles from the matrix. The plastic deformation criterion of the nucleation of voids is accepted. The nucleation material function h depends on the equivalent plastic deformation $\bar{\epsilon}_p$. The second term in Eq. (2.9) is related to the growth mechanism. The growth material function g also depends on the equivalent plastic deformation $\bar{\epsilon}_p$. It is assumed for simplicity that the material functions $\mathbf{h} = h(\bar{\epsilon}_p, a_1, b_1, c_1)$ and $\mathbf{g} = g(\bar{\epsilon}_p, a_2, b_2, c_2)$ depend only on the equivalent plastic deformation $\bar{\epsilon}_p$ and the unknown parameters. It is assumed that the nucleation mechanism in (2.9) is controlled by the plastic strain only.

3.1. Constitutive relation for the porous elastic-plastic solids

The constitutive relation used by us has the form

$$D^p_{ij} = \frac{1}{H} P_{ij} Q_{kl} \overset{\triangledown}{\sigma}{}^{kl}, \qquad P_{ij} = \frac{\partial \phi}{\partial \sigma_{ij}}, \qquad Q_{kl} = \frac{\partial \phi}{\partial \sigma_{kl}}, \tag{3.1}$$

where $\overset{\triangledown}{\boldsymbol{\sigma}}$ is the Jaumann rate-of-change of Cauchy stress and ϕ is the classical Gurson plastic potential with q_1 and $q_2 = {q_1}^2$ parameters equal to 1. The flow potential is

$$\phi(\sigma, \xi, \bar{\sigma}) \; = \; \frac{\frac{3}{2} S_{ij} S_{ij}}{\bar{\sigma}^2} + 2 q_1 \xi \cosh\left(\frac{\sigma_{kk}}{2\bar{\sigma}}\right) - 1 - \left({q_1}^2 \xi\right)^2 = 0. \tag{3.2}$$

For plastic porous media with known yield function, the constitutive relation is expressed as follows:

$$D^p_{ij} = \frac{1}{H} \left(\frac{3 S_{ij}}{\bar{\sigma}^2} + \frac{\alpha}{\bar{\sigma}} \delta_{ij} \right) Q_{kl} \overset{\triangledown}{\sigma}{}^{kl}, \tag{3.3}$$

where $S_{ij} = \sigma_{ij} - \dfrac{1}{3} \sigma_{kk} \delta_{ij}$ and $\alpha = \xi \sinh\left(\dfrac{\sigma_{kk}}{2\bar{\sigma}}\right)$.

3.2. Porosity evolution at the neck

Making use of Eqs. (3.1) and (3.3), in Eq. (2.9) we obtain the following evolution equation:

$$\frac{\dot{\xi}}{\dot{\bar{\epsilon}}_{\mathrm{p}}} = \left[\mathbf{h} \frac{1}{1-\xi} \left(\lambda_1 \frac{\sigma_{xx}}{\sigma_{zz}} + \lambda_2 \frac{\sigma_{yy}}{\sigma_{zz}} + 1 \right) + \mathbf{g}(1-\xi)(\lambda_1 + \lambda_2 + 1) \right] \frac{1}{\sqrt{\lambda^*}}, \tag{3.4}$$

where $\bar{\epsilon}_p$ is the equivalent plastic strain, $\mathbf{h} = h(\bar{\epsilon}^p, a_1, b_1, c_1)$ and $\mathbf{g} = g(\bar{\epsilon}^p, a_2, b_2, c_2)$ are the material functions to be identified.

Constitutive relation allows to express the plastic rate $\mathbf{D}^p$ of the deformation tensor as a function of

$$\lambda_1 = \frac{D^p_{xx}}{D^p_{zz}}, \quad \lambda_2 = \frac{D^p_{yy}}{D^p_{zz}} \quad \text{and} \quad \lambda^* = \frac{2}{3}\Big[(\lambda_1)^2 + (\lambda_2)^2 + 1\Big].$$

Using relation (3.3) we conclude that λ_1, λ_2 are equal to

$$\lambda_1 = \lambda_2 = \frac{3S_{xx} + \bar{\sigma}\alpha}{3S_{zz} + \bar{\sigma}\alpha}. \tag{3.5}$$

The deviators S_{xx} and S_{zz} of the stress state and the hydrostatic part of the stress are expressed by

$$S_{xx} = \sigma_{xx} - \frac{1}{3}\sigma_{kk}\ , \quad S_{zz} = \sigma_{zz} - \frac{1}{3}\sigma_{kk}\ , \quad \sigma_{kk} = \sigma_{xx} + \sigma_{yy} + \sigma_{zz}.$$

3.3. Stress state at the neck

We employ BRIDGMAN's [1] solution for the stress state at the center of minimum section of the tensile cylindrical sample. It has been obtained due to the assumption of uniform deformation of the elements in the minimum section, implying that the circumferential strain rate D^p_{yy} is equal to radial strain rate D^p_{xx} in the minimum section (cf. CHAKRABARTY [3]) p. 161), inserting this equality in the equilibrium equations and combining with the yield condition

$$\begin{aligned} \sigma_{xx} &= \sigma_{yy} = \bar{\sigma}\ln\left(\frac{1}{2}\frac{R}{\rho_R} + 1\right) \\ \sigma_{zz} &= \bar{\sigma}\left(1 + \ln\left(\frac{1}{2}\frac{R}{\rho_R} + 1\right)\right) \end{aligned} \qquad \text{for} \quad x,\ y,\ z = 0. \tag{3.6}$$

The analytical expression for the stress depends on the matrix flow stress, $\bar{\sigma}$ and the geometry of the neck, i.e. on the ratio $\dfrac{R}{\rho_R}$, where R is the radius of the minimum section and ρ_R is the neck contour radius. The behaviour of the matrix material is represented by a piecewise power law of the form $\bar{\sigma} = \sigma_y \cdot (\bar{\epsilon}_p/\epsilon_y)^{\mathrm{N}}$. Here σ_y is the yield stress in uniaxial tension, ϵ_y is the yield strain of the matrix material and N is the matrix strain hardening exponent, e.g. for carbon steel $\sigma_y = 175.0$ MPa, $\epsilon_y = 0.001$ and $\mathrm{N} = 0.18$. Similarly as in SAJE,

PAN and NEEDLEMAN [2] it is assumed that

$$\frac{R}{\rho_R} = 0.833(\bar{\epsilon}_p - 0.18), \qquad \text{for } \bar{\epsilon}_p \geq 0.18;$$
$$\frac{R}{\rho_R} = 0.0, \qquad \text{for } \bar{\epsilon}_p < 0.18. \tag{3.7}$$

Taking Eqs. (6.) into account in the Bridgman solution, we obtain for axisymmetric tension

$$\frac{\sigma_{xx}}{\sigma_{zz}} = \frac{\sigma_{yy}}{\sigma_{zz}} = \lambda, \tag{3.8}$$

where

$$\lambda = \ln\left(\frac{1}{2}\frac{R}{\rho_R} + 1\right) \Big/ \left(1 + \ln\left(\frac{1}{2}\frac{R}{\rho_R} + 1\right)\right). \tag{3.9}$$

Furthermore, we have assumed the constitutive relation for the porous plastic solids introduced in the form of Eq. (3.1) by GURSON [11].

Using this relation we can determine λ_1 and λ_2

$$\lambda_1 = \lambda_2 = (3S_{xx} + \bar{\sigma}\alpha)/(3S_{zz} + \bar{\sigma}\alpha). \tag{3.10}$$

4. The form of material functions

This section contains formulae of the material functions which we have used for identification. There exist certain requirements which the shape of the material function h has to satisfy. We have selected the form of material functions $\mathbf{h} = h(\bar{\epsilon}^p, a_1, b_1, c_1)$ and $\mathbf{g} = g(\bar{\epsilon}^p, a_1, b_1, c_1)$ following two rules:

- We prefer the formulae with known mechanical interpretation.
- We prefer the simplest form of them.

We started trying to follow the ideas of CHU and NEEDLEMAN [40]. So, as the first type of the function, the Gauss normal distribution function for function h was applied

$$h_1(\bar{\epsilon}_p, a_1, b_1, c_1) = \frac{a_1}{b_1\sqrt{2\pi}} \exp\left(-\frac{1}{2}\left[\frac{\bar{\epsilon}_p - c_1}{b_1}\right]^2\right), \tag{4.1}$$

where a_1, b_1, c_1 are the unknown parameters. All of these parameters have their mechanical meaning. Namely, a_1 denotes the maximum value of the porosity parameter, b_1 is the width of the voids distribution region and c_1 represents

the value of the equivalent plastic strain $\bar{\epsilon}_p$ at the moment when the porosity parameter reaches its maximal value.

In the previous studies, cf. NOWAK and STACHURSKI [30], we have also used two other forms of the material functions h:

$$h_2 = a_1(\bar{\epsilon}_p)^{b_1}\exp(c_1\bar{\epsilon}_p), \tag{4.2}$$

$$h_3 = a_1[1+\tanh(b_1\bar{\epsilon}_p + c_1)]. \tag{4.3}$$

In the current investigation we have decided to neglect h_2 since it was worse than the two other nucleation material functions.

The second material function g describing the growth of microvoids must be uniformly equal to 1 when initial void or voids are isolated in an unbounded matrix. It means that voids do not interact, no nucleation of new voids and no coalescence of voids in the growth process are considered. These three phenomena are closely interrelated and can occur simultaneously. The material function $g \equiv 1$ is well verified when only the growth process of isolated voids takes place. It is preferred for incompressible "strong" metals in the room temperature. However, it is so in such cases when the growth of voids is the main effect and the nucleation of voids is neglected or included without taking into account their mutual interaction. Some recent experimental papers dealing with plastic compressibility of metals (e.g. GOTOH and YAMASHITA [31]) pointed out that the evolution of voids in the Gurson model requires some improvements. Their identification results for the uniaxial tension and equi-biaxial tension support the opinion that $g \equiv \text{const} = \alpha \neq 1$. Our growth function g results from the volume change of the already existing voids and the newly nucleated voids and interactions among them, while the nucleation function h expresses nucleation of new voids, controlled by plastic deformation only. We set $(\dot{\xi}_{\text{growth}}/(1-\xi) = g\dot{E}^p_{kk}$, and g is the fraction due to void growth within the total volume strain rate $\dot{E}^p_{kk}$.

In our analysis this function g is not necessarily constant. As the first form of the g function, the following formula (as in PERZYNA and NOWAK [37]) was used:

$$g_1(\bar{\epsilon}_p, a_2, b_2, c_2) = a_2 \exp\left[b_2\,(\bar{\epsilon}_p)^{c_2}\right]. \tag{4.4}$$

Unfortunately, in this case, the mechanical interpretation of the unknown parameters a_2, b_2 and c_2 is not so clear.

The identification was also carried out with five other different forms of the material function g

$$g_2 = a_2\sqrt{(\bar{\epsilon}_p)^2 + b_2(\bar{\epsilon}_p) + c_2}, \tag{4.5}$$

$$g_3 = \frac{a_2}{b_2 - \bar{\epsilon}_p}, \tag{4.6}$$

$$g_4 = 1, \tag{4.7}$$

$$g_5 = a_2, \tag{4.8}$$

$$g_6 = a_2 + b_2 \cdot \bar{\epsilon}_p. \tag{4.9}$$

Tables 1a summarizes notation of the cases for the total porosity model and Table 1b – for the separated porosity model. For instance, Case A1 denotes selection of h_1 and g_1. This means that we apply the normal Gauss distribution function as the nucleation material function h and the exponential function as the growth material function g. Case B1 corresponds to h_2 and g_1 and so on.

Table 1. Summary of notations for a) the total porosity model; b) the separated porosity model.

	g–function					
	g_1	g_2	g_3	g_4	g_5	g_6
h_1	A1	A2	A3	A4	A5	A6
h_3	C1	C2	C3	C4	C5	C6

	g–function					
	g_1	g_2	g_3	g_4	g_5	g_6
h_1	DA1	DA2	DA3	DA4	DA5	DA6
h_3	DC1	DC2	DC3	DC4	DC5	DC6

The corresponding cases for the separated porosity model are denoted similarly. The only difference is the addition of capital D in front of the case symbol. Hence, for example DA1 means the use of functions h_1 and g_1.

We have maintained the same order of notations in the separated and total porosity models to simplify the comparison of identification results in both cases. The tables of results for the total porosity model are presented in the Appendix, Subsec. A1 and for the separated porosity model in Subsec. A2.

5. Criteria for models selection

Mathematical models are selected by evaluating how well each one fits the experimental data. The model that provides the best fit (i.e. the smallest deviation) is preferred. Usually a model with many free parameters can provide a better fit to the data sample than a model with few parameters. Our aim is to select the model that is simple and fits well. Therefore we should find a compromise between simplicity and fitting. It is necessary to make selection in the set of the nested and non-nested models. The first are discussed in the following Subsec. 5.1 while the latter are presented in the Subsec. 5.2.

5.1. Criteria for nested models selection

We decided to use the Akaike information criterion (AIC) and the final prediction error criterion (FPE) to discriminate between two or more nested mod-

els. Those two criteria penalize a model more as the number of parameters n increases. Below are the formulae allowing to calculate their values.

- Akaike's information criterion AIC (SÖDERSTRÖM and STOICA [42], p. 442)

$$\text{AIC} = M * \ln V_M(\hat{\mathbf{x}}) + 2 * n, \tag{5.1}$$

where: M is the number of observations, $\hat{\mathbf{x}}$ is the set of the model parameters, n denotes their number and $V_M(\hat{\mathbf{x}})$ is the quadratic loss function

$$V_M(\hat{\mathbf{x}}) = \sum_{i=1}^{M} \left(Y_i - \tilde{Y}_i\right)^2, \tag{5.2}$$

where Y_i and $\tilde{Y}_i$ have the same meaning as those expressed in Sec. 2.2 below the formula (4.8).

- Final prediction error criterion (FPE) (SÖDERSTRÖM and STOICA [42], p. 444)

$$\text{FPE} = V_M(\hat{\mathbf{x}}) * \frac{1 + n/M}{1 - n/M}. \tag{5.3}$$

The meaning of the symbols is the same as in the Akaike formula.

5.2. Vuong test for discriminating between the rival nonnested models

There exist several tests for discriminating between the nonnested models (for instance: Cox test, Vuong test, Bayes factors, F test, J test, JA test) (see CLARKE [5], MCALEER [6], VUONG [46]). We have considered the use of the Cox and Vuong Tests. The Cox test is harder to perform than the Vuong test. It requires many extra simulations to calculate its value. Furthermore, it may reject both of the two compared models without any decision. The Vuong test is the easiest to perform; it is only necessary to calculate the difference in the average log-likelihoods and calculation of the normalization. It requires neither simulation nor any prior information. Vuong test never leaves us without any answer. It allows to select the best model even from a set of bad nonnested models.

The null hypothesis in the Vuong test is that the compared models H_1 and H_2 are equivalent. The actual (approximate) test is:

$$\text{under } H_0 : \frac{LR_M(\hat{x}^1_M, \hat{x}^2_M)}{(\sqrt{M}) \cdot \hat{\omega}_M} \longrightarrow N(0,1), \tag{5.4}$$

$$\text{under } H_1 : \frac{LR_M(\hat{x}^1_M, \hat{x}^2_M)}{(\sqrt{M}) \cdot \hat{\omega}_M} \longrightarrow +\infty, \tag{5.5}$$

$$\text{under } H_2 : \frac{LR_M(\hat{x}^1_M, \hat{x}^2_M)}{(\sqrt{M}) \cdot \hat{\omega}_M} \longrightarrow -\infty, \tag{5.6}$$

where

$$LR_M(\hat{x}^1_M, \hat{x}^2_M) \equiv L^1_M(\hat{x}^1_M) - L^2_M(\hat{x}^2_M), \tag{5.7}$$

$$\hat{\omega}^2_M \equiv \frac{1}{M}\sum_{i=1}^{M}\left[\ln\frac{f_1(Y_i|X_i;\hat{x}^1_M)}{f_2(Y_i|Z_i;\hat{x}^2_M)}\right]^2 - \left[\frac{1}{M}\sum_{i=1}^{M}\ln\frac{f_1(Y_i|X_i;\hat{x}^1_M)}{f_2(Y_i|Z_i;\hat{x}^2_M)}\right]^2. \tag{5.8}$$

Here $f_1(Y_t|X_t;\hat{x}^1_M)$ ($f_2(Y_t|X_t;\hat{x}^2_M)$) denotes the true conditional density of Y_t given X_t for the first (second) model with parameters equal to $\hat{x}^1_M$ ($\hat{x}^2_M$) – the estimated values of x^1 (x^2). Our models have different numbers of parameters. Therefore, following CLARKE [5] we have adjusted the log-likelihood-ratio statistic

$$\widehat{\mathrm{LR}}_M(\hat{x}^1_M, \hat{x}^2_M) = \mathrm{LR}_M(\hat{x}^1_M, \hat{x}^2_M) - \left[\left(\frac{n1}{2}\right)\ln(M) - \left(\frac{n2}{2}\right)\ln(M)\right], \tag{5.9}$$

where $n1$ and $n2$ are the numbers of parameters in models 1 and 2, respectively.

5.3. Selection criteria for models with separated porosities

In cases corresponding to the model with separated nucleation and growth porosity (with the prefix "D", see Table 1), all statistical quantities together with the Akaike's and FPE information criteria are calculated for the separated cases treated as total (i. e. after summing up the outputs) to make them comparable with the corresponding total case. Those criteria are used to discriminate between the rival nested models. Furthermore, it should be stressed that only a few of our models form groups of nested models. Therefore we use only a part of them in the analysis.

6. Description of fisher's experimental data used for estimation

In J.R. Fisher's experimental investigation two carbon steels with 0.17 (type B) and 0.44 (type W) weight percent carbon, respectively, were used for the quantitative studies of microvoid nucleation and growth. All testing was done at the room temperature. Metallographic observations were made on both undeformed and deformed specimens using both optical and electron microscopy. For each specimen, a series of transverse sections was prepared corresponding to successively smaller axial distances from the minimum cross-section. Each new section was obtained by grinding to the next premarked position and thus the previous sections were destroyed. Therefore, all data required from a given section

had to be obtained before preparation of the succeeding one. Each section was carefully polished and etched after preliminary use of various grades of abrasive papers. The microstructural parameters were determined in both the deformed and undeformed specimens. For the deformed specimens the areal density of voids, η_A, and the volume fraction of voids, ξ, were obtained from transverse sections by standard metallographic techniques performed on scanning electron micrographs taken at a magnification of 2000 times. It is observed in Fisher's experiment that the voids tended to have elliptical cross-sections similar to those of the particles, as might be expected since the particles were nucleation sites for these voids.

The total volume fraction of voids, ξ, and the nucleation part of volume fraction of voids, ξ^n, obtained by FISHER [7], are plotted as functions of equivalent plastic strain $\bar{\epsilon}_p$ in Fig. 1. This measure of voids is used in our analysis in Sec. 2.3, it is worth to separate the nucleation part from the full measure of ξ. As in PERZYNA and NOWAK [37], the resulting diagrams of the nucleation part of ξ^n and the growth part of ξ^g versus $\bar{\epsilon}_p$ are shown also in Fig. 1.

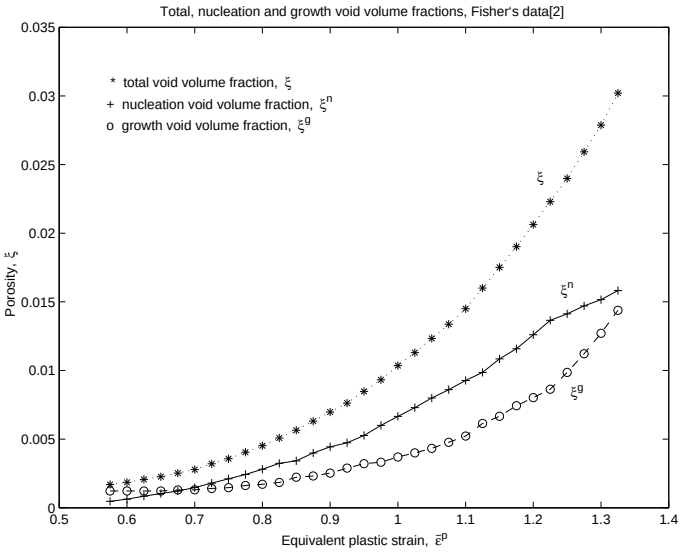

FIG. 1. Total void volume fraction, ξ, the nucleation volume void fraction, ξ^n (data from FISHER [7] for the $B1$-type steel) and the calculated growth volume void fraction, ξ^g, as the functions of equivalent plastic strain, $\bar{\epsilon_p}$.

The following observations could be drawn from the Fisher's experimental work:

- Voids are generally associated with particles of greater than average size. They rarely form at very small, isolated particles, even for the severe state of deformation which exists in the neck of a tensile specimen.

- Particles situated on ferrite grain boundaries are favoured sites for the nucleation of voids.
- Voids often form by decohesion of the interfaces of particles which are closely spaced along the tensile axis.
- The maximum gradient in the void nucleation profile occurs at strains of $\bar{\epsilon}_p = 1.15$ and $\bar{\epsilon}_p = 0.80$ for B and W-type specimens respectively.
- Voids elongate in the tensile direction but maintain elliptical cross-sections, indicating that plastic hole growth, and not ferrite grain boundary separation, dictates the final void geometry.
- Non-equiaxial or irregularly shaped cementite particles are often subject to internal fracture. The resulting cracks tend to be oriented normally to the tensile direction and may sometimes be associated with boundaries between contiguous particles.

In this work, the thorough analysis of the data set was omitted since we have decided to concentrate on the computational aspects of the problem of parameter estimation. We were interested in the question of whether it is in fact the global optimization problem. Furthermore, we wanted to obtain a decisive answer to the question of whether the assumed model does fit at all the given data set.

7. Numerical methods

Our earlier experience with the porosity model [28] has proved the existence of many local minima in our problem. Therefore we have used for calculations our own implementation (standard ANSI C language) of the global minimization method of BOENDER, RINNOY KAN, TIMMER and STROUGIE [43] in the form presented in (standard ANSI C language) of the global minimization method of TÖRN and ŽILINSKAS [44]. The details of the method are presented in (standard ANSI C language) of the global minimization method of NOWAK and STACHURSKI [28]. In this paper we shall restrict it to a necessary minimum. To simplify the presentation of the computational algorithm, let us assume that we consider the following optimization problem:

$$\min_{\mathbf{x} \in V \subset R^n} f(\mathbf{x}), \tag{7.1}$$

where: vector $\mathbf{x}^T = (a_1, b_1, c_1, a_2, b_2, c_2\ )$ ($\mathbf{x}^T$ – denotes the transposition of the column vector $\mathbf{x}$), $n = 6$ (sometimes 3 or 5) and V denotes the set of feasible values of parameters.

Implemented by us the global optimization method of BOENDER, RINNOY KAN, TIMMER and STROUGIE [43] belongs to the group of the so-called clustering methods and is a combination of sampling, clustering and local search.

Detailed structure of the algorithm:

Step 0. Select N – number of sample points generated in one phase and g-fraction of the sample points with the smallest function values. X^+ – the set of all local minima found so far; $X1$ – the set of sample points leading to a minimum $\hat{\mathbf{x}} \in X^+$. Choose parameter $e_{C1} > 0$ used in the clusterization.

Step 1. Select N randomly generated points $\mathbf{x}^1, \mathbf{x}^2, \cdots, \mathbf{x}^N$. Let $f^i = f(\mathbf{x}^i)$ for $i = 1, \cdots, N$.

Step 2. Construct the transformed sample by taking the fraction g of the lowest points of the current sample, performing one step of the steepest descent method and replacing those points by the resulting points. Drop the rest of the points.

Step 3. Apply the clustering procedure to the transformed sample. The elements of X^+ (set of global points – local minima found up till now) are first chosen as seed points followed by the elements of $X1$ (set of sample points leading to a minimum $\hat{\mathbf{x}} \in X^+$). If all points $\mathbf{x}^1, \mathbf{x}^2, \cdots, \mathbf{x}^{N^+}$ are classified then STOP, otherwise go to the next step.

Step 4. For $i = 1, \cdots, N^+$, if $\mathbf{x}^i$ is classified neither to X^+ nor to $X1$ then

a) apply the local search procedure starting from $\mathbf{x}^i$ to obtain $\mathbf{x}^{i+}$.

b) if $\mathbf{x}^{i+} \in X^+$ then add $\mathbf{x}^i$ to $X1$ (new seed point leading to an existing minimum),

c) if $\mathbf{x}^{i+} \notin X^+$ ($\mathbf{x}^{i+}$ is a new local minimum) then add $\mathbf{x}^{i+}$ to X^+ and $\mathbf{x}^i$ to $X1$.

Step 5. Return to Step 1.

The described global optimization method characterizes convergence with probability one as in any other involvd stochasticity. Generally, involving stochastic elements, one sacrifices the possibility of an absolute guarantee of success. One can only get, under mild assumptions on the minimized function and the sampling distribution, a result that the probability of sampling a point in the neighbourhood of the global optimum x* tends to 1 if the number of sample points in the global phase is increased. If the sampling distribution is uniform over and function f is continuous, then the sample point with lowest function value tends to a point with minimal function value with probability 1.

Hence, the global phase could asymptotically guarantee the success. In clustering methods one tries to increase efficiency by including a local search phase. As the stopping criterion we require fulfillment of one of the following conditions:

- all points from the transformed sample could be classified,
- either the number of local minima found or the number of points leading to a minimum is greater than their maximal permitted number,
- either the number of global minima found or the number of global seed points (i.e. sampling points leading towards a global minimum) is greater than the user-defined maximal value.

Locally we have used the BFGS quasi-Newton method with the numerical gradient estimation. The BFGS method is an unconstrained optimisation method; however, in our implementation we have introduced box constraints on the parameters. Our local minimizer makes use of a directional minimization method combining three different approaches – via quadratic approximations along the search direction, cubic approximations and bisection. Paper [28] presents their details. The third computational aspect is connected with the ordinary differential equation to be solved. It contains singularity in its right-hand side and it leads to difficulties with its numerical integration. The Runge–Kutta methods with automatic step-size selection has locked themselves in a kind of cycle. Therefore we have decided to choose the Rosenbrock method for stiff differential equations (see Numerical Recipes [45]).

8. Numerical results

In this section the results of parameter estimation are presented. Their presentation is restricted to only one minimum corresponding to the current loss-function value. Other local minima found are neglected.

Our aim in considering various forms of material functions was to obtain the "best" fitting of the model to the data in the sense that we find the parameters ensuring the smallest value of the analysed loss function (4.11) or (2.13), respectively. Furthermore, in all cases it is necessary to impose some bounds on the parameters to assure their appropriate mechanical interpretation and to avoid overflows in calculations (specially for the g function). In our computations we have used the following strategy: at the beginning, broad ranges of the feasible parameters were assumed. In each case and current choice of the loss function we have started our computations assuming at the beginning a broad range of feasible parameters. For instance, in Cases A1, A2 and A3 and with the least squares loss function, we have taken

$$\begin{aligned}
\text{A1:}\quad & 0.01 \le a_1 \le 0.05, \quad 0.1 \le b_1 \le 0.6, \quad 0.9 \le c_1 \le 1.3,\\
& 1.0 \le a_2 \le 1.5, \quad 0.01 \le b_2 \le 0.3, \quad 0.01 \le c_2 \le 0.6,\\
\text{A2:}\quad & 0.01 \le a_1 \le 0.1, \quad 0.1 \le b_1 \le 0.5, \quad 1.0 \le c_1 \le 1.3,\\
& 0.1 \le a_2 \le 0.6, \quad 0.5 \le b_2 \le 1.2, \quad 0.8 \le c_2 \le 1.8,\\
\text{A3:}\quad & 0.01 \le a_1 \le 0.1, \quad 0.1 \le b_1 \le 1.0, \quad 1.0 \le c_1 \le 1.3,\\
& 1.5 \le a_2 \le 3.0, \quad 2.5 \le b_2 \le 5.0.
\end{aligned}$$

At each such main step we have found several local optima. Many of them had some variables lying on their bounds. Because of that we have adopted special strategy consisting in subsequent minimizations with restricted range

of parameters. It gave us an opportunity to better explore the whole range of parameters we were interested in. The second and very important reason for such a strategy was the large computational effort and memory requirements to store many local minima and points leading towards them if we decided to run the program assuming an excessively broad range of parameters. The third and not less important reason were the numerical difficulties encountered in integration of the differential equation. Its right-hand side contains a singularity and is very sensitive, even to relatively small changes in some parameters. It was sometimes impossible to satisfy the accuracy requirements in the double precision arithmetic of the workstation.

In our calculations each case corresponds to a different combination of the material functions h and g. Every case was run with four different loss functions ϑ_i (cf. Sec. 2.1) The Huber and Beaton and Tuckey loss functions were used with the threshold $A = 10^{-8}$. Our computational strategy may be summarized as follows:

- At the beginning, broad ranges of the feasible parameters were assumed.
- At the next steps, small intervals containing the previously found optimal values of parameters as their new feasible ranges are selected.
- At each such main step we have found several local optima. Many of them had some variables lying on their bounds. Because of that we have adopted a special strategy consisting in subsequent minimizations with restricted ranges of parameters.

Information collected in the Tables below was investigated to select the best model found with the aid of any particular loss function. The selection was carried out according to the following rules:

- select, on the basis of the Akaike or FPE information criteria, the best model from any group with the $g \equiv 1$, g being the estimated constant and g linear and one particular form of the h function, for instance A4, A5 and A6;
- select using the Vuong criterion the best representative of any group with one h formula and all other forms of g including linear g (for instance, the first group consists of A2 and A3).

Models selected in two previous steps independently for the total and separated cases are pairwise compared via the Vuong test. Due to the lack of space we have decided to omit some tables for the separated model cases. Furthermore, they are generally worse than the corresponding total cases in the sense that the data fitting is worse.

8.1. Results for AIC and FPE tests for the total porosity model

Tables are organized as follows. Table 2 summarizes identification results for the total porosity model with variable growth material function.

Table 2. Identified parameters and fitting errors for the cases A1–A3, A6, C1–C3, C6 h – nucleation functions with a_1, b_1 and c_1; g – growth functions with a_2, b_2 and c_2.

Function	Case	a_1	b_1	c_1	a_2	b_2	c_2	f
F_1		0.017201	0.297427	1.095775	1.134962	0.138219	0.493378	1.65712212e-7
F_2	A1	0.018690	0.300661	1.113979	1.118014	0.122462	0.408996	2.37068266e-7
F_3		0.015417	0.285030	1.069471	1.157578	0.152573	0.481765	1.65665286e-7
F_4		0.014276	0.275759	1.047057	1.041307	0.274952	0.441723	1.66603238e-3
F_1		0.021122	0.304899	1.117584	0.577458	1.091203	1.687886	1.65244609e-7
F_2	A2	0.024416	0.347778	1.162565	0.588316	1.123116	1.345267	3.64393058e-7
F_3		0.030403	0.342234	1.211028	0.521447	1.055361	1.248056	1.70679157e-7
F_4		0.018018	0.284599	1.075274	0.652583	0.849635	1.444798	1.66429333e-3
F_1		0.024351	0.317042	1.151407	2.456718	3.354722		1.65990605e-7
F_2	A3	0.026001	0.329372	1.158489	1.551271	2.587062		2.50690905e-7
F_3		0.023815	0.311174	1.141462	2.249023	3.168313		1.67147464e-7
F_4		0.022060	0.299496	1.113956	1.775550	2.704330		1.66370570e-3
F_1		0.022623	0.317819	1.143767	0.776960	0.345368		1.66474086e-7
F_2	A6	0.028400	0.395088	1.258077	0.950536	0.223465		7.34746418e-7
F_3		0.021389	0.311633	1.129490	0.814343	0.333191		1.67375842e-7
F_4		0.015910	0.274087	1.055807	0.909310	0.362792		1.67399047e-3
F_1		0.020692	2.950418	-2.594659	0.986654	0.037083	0.172817	1.77862805e-7
F_2	C1	0.015305	2.848600	-2.342232	0.996927	0.197966	0.248658	5.00161040e-7
F_3		0.018024	3.158168	-2.664735	1.051133	0.037578	0.242513	1.69917395e-7
F_4		0.021539	3.056008	-2.683907	0.933438	0.038638	0.199740	1.76929149e-3
F_1		0.026138	2.812440	-2.566309	0.439508	0.764393	1.524417	1.82233773e-7
F_2	C2	0.028975	2.559279	-2.444271	0.424864	0.748597	1.647193	2.38760427e-7
F_3		0.024722	2.851439	-2.565044	0.451971	0.733190	1.667110	1.81540589e-7
F_4		0.033142	2.708107	-2.611123	0.334805	0.882942	1.636062	1.87906702e-3
F_1		0.037502	2.539226	-2.565301	1.889970	4.124723		2.12654576e-7
F_2	C3	0.028378	2.383227	-2.277388	1.393423	2.781586		5.02547881e-7
F_3		0.037924	2.551824	-2.579912	1.870462	4.158467		2.14271041e-7
F_4		0.019951	3.518412	-2.905076	1.742845	2.968712		1.73245751e-3
F_1		0.026199	2.816344	-2.564785	0.419120	0.368563		1.81211940e-7
F_2	C6	0.028805	2.569758	-2.455680	0.519015	0.279190		2.29954122e-7
F_3		0.026236	2.743705	-2.538666	0.632538	0.207441		1.87897483e-7
F_4		0.025053	2.897769	-2.614352	0.597552	0.232755		1.81161333e-3

To each case (corresponding to the particular choice of the material function h and g) we have assigned four lines corresponding to different forms of the loss function. Each line contains the estimated material functions parameters and the corresponding loss function value.

Table 3 presents the same information for the cases with a constant growth function g.

Table 3. Identified parameters and fitting errors for the cases A4, A5, C4, C5 h – nucleation functions with a_1, b_1 and c_1; g - constant growth function with $a_2 = 1$ and a_2 estimated.

Function	Case	a_1	b_1	c_1	a_2	f
F_1		0.036075	0.372862	1.294913	1.0	1.88089923e-7
F_2	A4	0.032938	0.347390	1.253591	1.0	3.99490475e-7
F_3		0.036058	0.372840	1.294757	1.0	1.88104823e-7
F_4		0.032697	0.352285	1.254021	1.0	1.78032600e-3
F_1		0.023793	0.337251	1.186571	1.191906	1.75387665e-7
F_2	A5	0.015550	0.291825	1.089597	1.385578	4.00855106e-7
F_3		0.014863	0.286185	1.068574	1.384094	1.65966325e-7
F_4		0.013065	0.271715	1.039402	1.437740	1.68082307e-3
F_1		0.021889	2.861803	-2.563658	1.0	1.81808536e-7
F_2	C4	0.023382	2.671133	-2.472136	1.0	2.32037301e-7
F_3		0.021786	2.875537	-2.569953	1.0	1.81269725e-7
F_4		0.020544	3.120742	-2.707662	1.0	1.76710774e-3
F_1		0.022198	2.851664	-2.564125	0.992077	1.82568420e-7
F_2	C5	0.018675	2.760810	-2.408759	1.121656	2.66220454e-7
F_3		0.022114	2.822994	-2.541973	1.0	1.84793577e-7
F_4		0.026775	2.821888	-2.629231	0.845772	1.83766355e-3

The corresponding statistical information criteria, i.e. Akaike and FPE, have selected the same models. Therefore the paper contains exclusively the FPE criterion values presented as bar plots in Fig. 2.

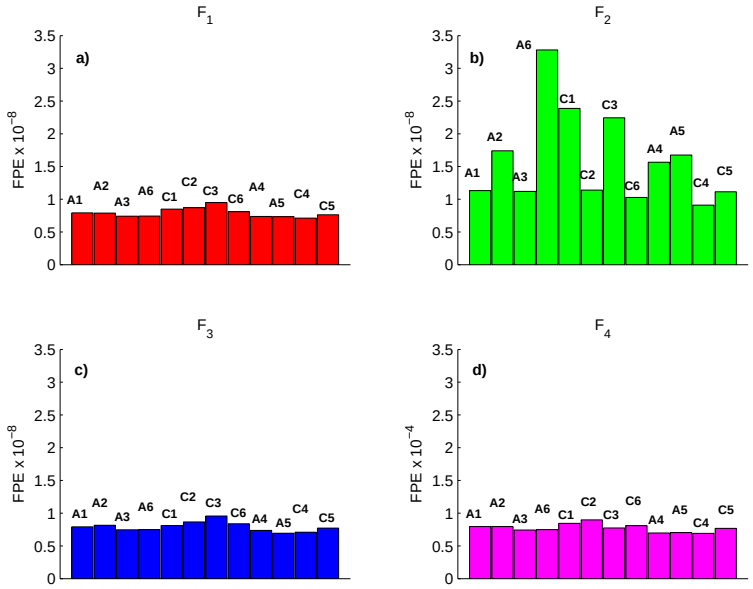

FIG. 2. Values of the FPE information criterion (four different cases corresponding to particular loss functions) – for total models.

8.2. Results for AIC and FPE tests in case of separated models

For the separated models we have decided to omit tables containing the identified parameter values and the corresponding fitting errors. The fitting error is the sum of deviations of two outputs – nucleation and growth porosity. In that case it is of magnitude 10^{-6}.

The statistical indicators are also relatively good. Akaike and FPE indicators point out that the linear g (i.e. DA6 and DC6) are the best ones in all groups. The results are collected in Fig. 3.

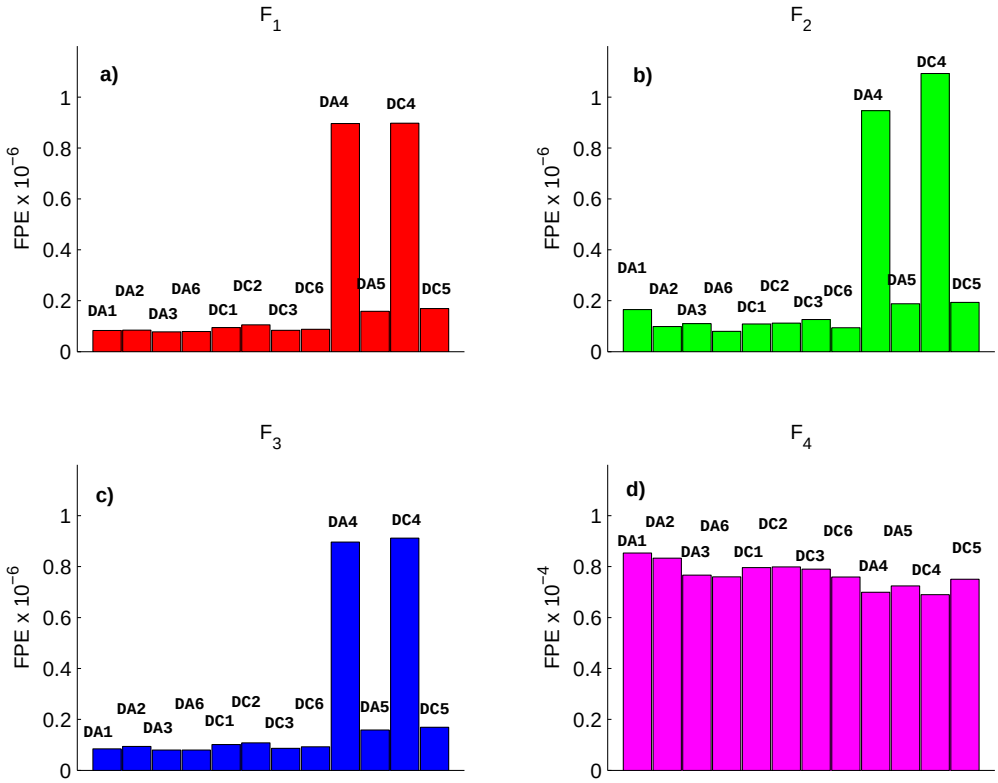

FIG. 3. Values of the FPE information criterion (four different cases corresponding to particular loss functions) – for separated models.

8.3. Results for Vuong test for the total porosity model

Analysis of the data in Fig. 2 proves that A5 (with h–normal distribution and g-estimated constant) is the best one in the group of nested models A4, A5 and A6 (statement valid for loss functions F_1 and F_3). For loss functions F_2

and F_4, model A4 (with h–normal distribution and $g \equiv 1$) is the best. Similarly Fig. 3 points C4 (with h–tangent function and $g \equiv 1$) as the best among C4, C5 and C6. This statement is true for all loss functions.

The best models selected by means of the Akaike and FPE tests for each group were further compared using the Vuong test with the non-nested models. The Vuong test results are presented graphically on Fig. 4. Fig. 4a) containing Vuong's test values for mutual comparison of models A2, A3, A5, C2, C3, C4 obtained by means of the loss function F_1. There are six groups of bars corresponding to the six models that are compared. Each group presents Vuong test values for proving the hypothesis that the current model is better than any from the others. For instance, the first group in Fig. 4a contains the results of testing model A2 versus A3, A5, C2, C3, C4. Bars above the zero level indicate that the current model is better than the compared model (for instance, the first group shows that A2 is better than C2 and C3 and worse than the other models A3, A5 and C4).

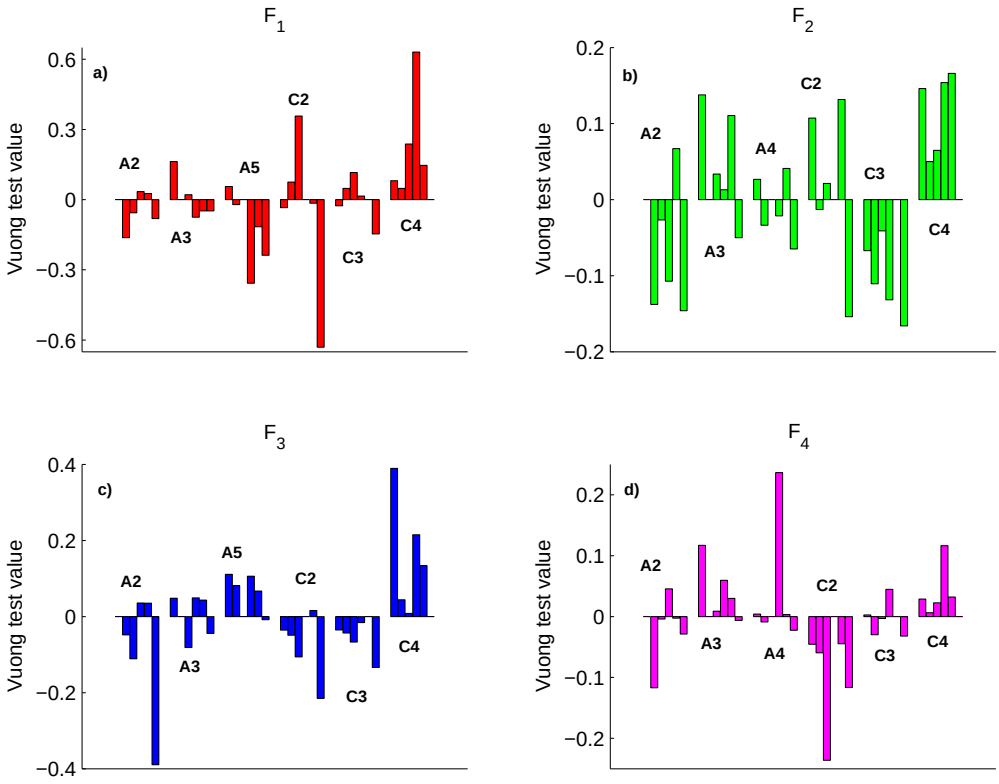

FIG. 4. Vuong test values best models from particular groups (four different cases corresponding to particular loss functions) – for total models.

8.4. Results for Vuong test in case of separated models

The Vuong test results for separated models, similarly as in the previous subsection, are depicted graphically in Fig. 5. The FPE criterion has specified DA6 as the best from the group of nested models DA4, DA5, DA6, and DC6 as the best one among DC4, DC5, DC6. This conclusion is valid for all loss functions ($F1 - -F4$) and therefore model DA6 was compared against DA2 and DA3 (DC6 versus DC2 and DC3). Figure 5 contains the results of mutual comparison of models DA2, DA3, DA6 and DC2, DC3, DC6.

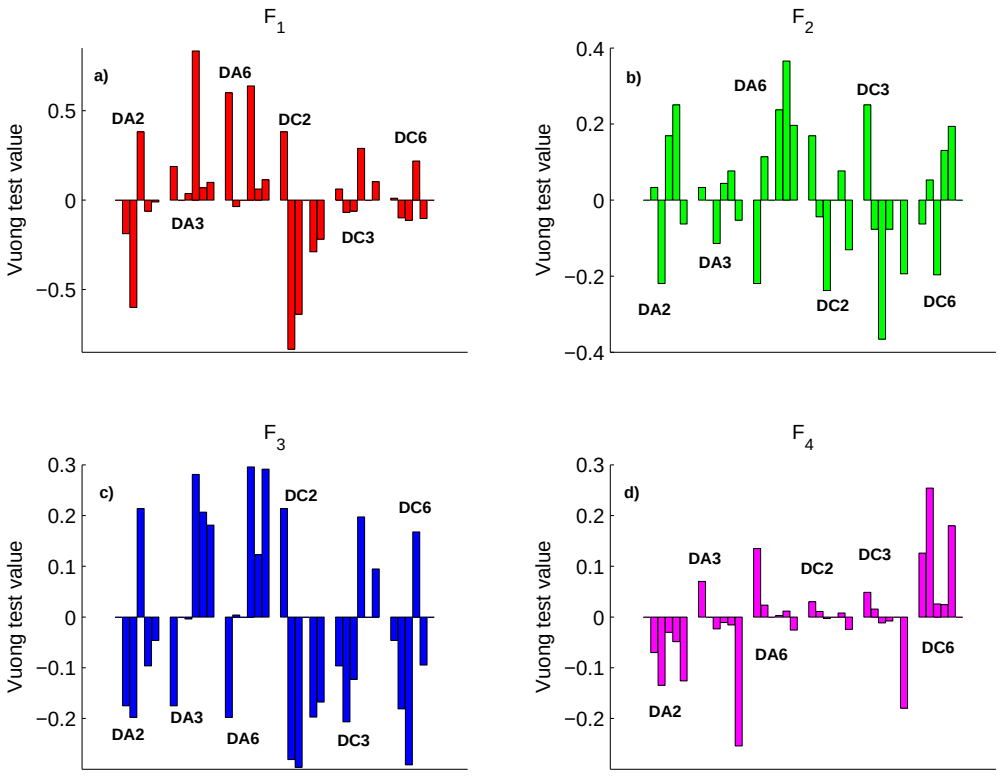

FIG. 5. Vuong test values best models from particular groups (four different cases corresponding to particular loss functions) – for separated models.

9. Analysis of the identification results

The current section contains analysis for results presented in Sec. 8. for the total and separated porosity models. Analysis in the separated porosity model is similar.

We have carried out two separate variants of numerical experiment with the total porosity model. The first one concerned the case with variable shapes of both material functions. The estimation results are collected in Table 2 (g-function takes forms g_1, g_2, g_3 and g_6 specified in Sec. 4). In the second case we have assumed a constant growth material function g (we have tested two variants – the first one with $g \equiv 1$ and the second one with an estimated value of that constant). Those results may be found in Table 2. Each particular form of g was run with h_1 and h_3. Therefore the above mentioned two cases contain many subcases. We have found many local minima in each run of the identification program. However, we present in Tables 2 and 3 only the best of them. Any particular choice of h and g is represented by four lines corresponding to different loss functions $F_1 - F_4$. Figure 2 presents graphically the corresponding statistical indicator FPE for total models. They were used for selection of the best model in the group of nested models.

Our earlier results with the quadratic loss function (see NOWAK and STACHURSKI [30]) has shown that for the varying growth material function g, the power-exponential function h_2 (see Eq. (4.2)) is the worst choice of the nucleation material function h. Estimation with other loss functions has supported that opinion and henceforth we have decided to omit the results for the h_2 in the tables. Two other nucleation material functions – normal distribution function h_1 (see Eq. (4.1)) and shifted hyperbolic tangent function h_3 (see Eq. (4.3)) are equally good. The mechanical interpretation of the normal distribution function parameters is easier. It was frequently used in the previous studies published in the literature. Therefore in our opinion, the normal distribution nucleation material function is a reasonable choice.

The large number of local minima found in all cases from that group led us to the conclusion that there exists a kind of an internal nonuniqueness in the total porosity model. Due to that observation we have decided to study the total porosity model with the growth material function $g \equiv 1$ (i.e. the form of the porosity model proposed by GURSON [11]) and g being an estimated constant.

The results for the constant growth function g collected in Table 3 show that the fitting error is of the same magnitude as in the corresponding cases with varying g function. They suggest that the constant growth material function $g \equiv 1$ used jointly with the nucleation material function h_3 (hyperbolic tangent function) is the best choice. This statement is valid for all loss functions except for F_3 where A_5 (model with the growth function equal to the estimated constant and the Gauss normal distribution as the nucleation material function) is better.

Vuong test for measures F_1 and F_3 selects model A5 with the Gauss distribution function as the nucleation material function and the estimated constant as the growth material function (from A2, A3 and A5) and C4 (with the shifted

hyperbolic tangent as the nucleation material function and the growth material function $g \equiv 1$) as the overall best model. Such a corollary follows from Fig. 4. However, it is interesting to stress that the fitting error obtained with the Gauss normal distribution as the h_1 function and g – an estimated constant, is better for model A5 with measures F_1, F_3 and F_4 than the C4 model – Table 3.

For measures F_2 and F_4 Vuong's test (see Fig. 4) selects model A3 with the Gauss normal distribution as the nucleation material function and the hyperbolic one as the growth material function (from models A2, A3 and A4) and once again as the overall best C4.

It is consistent with our previous results presented in NOWAK and STACHURSKI [30] for the least squares identification. It means that in our experiment, rejection of outliers (in the statistical indicators we weaken the influence of the observations larger than a given threshold value – the same as in the Huber robust loss function formula 2.4) has not changed the general conclusions.

The computations in a separated case were carried out in a similar manner as in the total porosity model. We have started with the varying growth function g and afterwards continued with the constant growth material function g. Akaike and FPE indicators point out that the linear growth material function g (i.e. DA6 and DC6) are the best ones in all groups. The FPE values are presented in Fig. 3. Fitting error in that case is of magnitude 10^{-6} and the statistical indicators are also relatively good. It should be stressed, however, that the fitting error in that case is the sum of deviations of two outputs – nucleation and growth porosity.

The Vuong test results for the separated model are presented in Fig. 5. It shows results of the mutual comparison of models DA2, DA3, DA6, DC2, DC3, DC6 identified with the aid of different loss functions, $F_1 - F_4$. For F_1 function, model DA3 (Gauss normal distribution as the nucleation material function and hyperbolic as the growth material function) is selected as the best one. For F_4 the Vuong test prefers model DC4 with the growth material function $g \equiv 1$ and the shifted hyperbolic tangent nucleation material function. It is interesting in that case that for the loss function F_2 and F_3, the Vuong test selects model DA6 (with g – linear and h – Gauss normal distribution). However, mean value of g is approximately equal to the constant found in model DA5 (with g – estimated constant), i.e. 0.8639 for function F_1, 0.8724 for F_2, 0.8637 for F_3, and 0.9438 for F_4, respectively. Similar property is observed for models assuming h_3 (Gauss normal distribution) as the nucleation material function.

We have observed a strong tendency to those constant values also for model DC6. Such phenomenon was not so clearly observed in the total porosity model, although the Vuong test value shows that the model C4 for measure F_3 is the best one and the model A5 (with h – the Gauss normal distribution function and g – an estimated constant) is only a bit worse. Value of the Vuong test for

measure F_3 of order 10^{-3} permits even to claim that C4 and A5 are equivalent. Figure 5 shows the FPE measures for separated porosity models obtained for constant material function g.

In the total porosity model every loss function finds the same "best model". Only the parameters values are slightly different. In the separated porosity model, the form of the best model is different, depending on the form of the loss function (see Table 4). In the separation porosity model we observe an important impact of the outliers (i.e. observations with large deviations) on the model selection. F_1 selects model DA3, F_2 and F_3 model, DA6 and F_4 model DC4.

Table 4. Best selected models.

Total porosity model					
Function	Best model	Selected material functions		f	Akaike
		g functions	h functions		
F_1	C4	g_4	h_3	1.81808534e-7	–581.5833
F_2	C4	g_4	h_3	2.32036369e-7	–574.0211
F_3	C4	g_4	h_3	1.81269747e-7	–581.6753
F_4	C4	g_4	h_3	1.76710326e-3	–296.9444

Separated porosity model					
Function	Best model	Selected material functions		f	Akaike
		g functions	h functions		
F_1	DA3	g_3	h_1	1.74196651e-6	–507.5290
F_2	DA6	g_6	h_1	1.79088112e-6	–506.6705
F_3	DA6	g_6	h_1	1.78622776e-6	–506.7511
F_4	DC4	g_4	h_3	1.76082030e-3	–297.0548

Calculations and analysis for the separated porosity model have been performed independently by us. The best models from both cases were compared by us by means of the Vuong test. That comparison has shown the superiority of the total porosity model.

10. Conclusions

Current analysis supports previously drawn conclusions (see NOWAK and STACHURSKI [30]), especially for the total porosity model. Model C4 (with the shifted hyperbolic tangent nucleation material function h_3 and the growth material function $g \equiv 1$) is the overall best for all loss functions. However, model A5 (h – Gauss normal distribution and g – estimated constant) is almost equally good (see Fig. 4). Therefore we claim similarly as before that it

is preferable to use h_1 – the Gauss normal distribution nucleation function and the estimated constat g at least in the total porosity case. The h_1 function is more suitable for mechanical interpretation. The conclusions are not so straightforward in the case of the separated porosity model. Introduction of the robust loss functions has totally changed the model selection results.

We have found several local minima in all cases. The best fitting error for the total porosity model is of the order 10^{-7}. However, the fitting error in other cases is only slightly larger. Of course, the corresponding material function parameters have different values. An open question is which local minimum found should be selected. It seems that in the total porosity model (when the voids nucleation and growth phenomena are simultaneously present), the constant material function $g \equiv 1$ as used by many researchers is an acceptable choice. However, we should stress that the identification procedure with $g = a_2$, where parameter a_2 was identified, has led to a bit different value of that constant.

In our opinion, the results obtained indicate that while modelling jointly the nucleation and growth of voids, it is reasonable to use the total porosity model with constant material function g. It seems that the constant should be different from the usually used value 1. We suggest its identification for each particular material. For the ductile steel this constant is probably near 0.86. It was somewhat unexpected by us and contrary to the common practice.

We recommend the use of the normal distribution function because it is easier to interpret its parameters in mechanical terms. We have observed equally good results for the shifted hyperbolic tangent function.

In all tested forms of the separated models we have also found several sets of parameters (local minima of the loss function) with the fitting errors close to the best one (within the range from 10^{-6} to 10^{-5}). The parameters are reasonable from the mechanical point of view. The model with the linear growth function g and the Gauss normal distribution nucleation function h has been selected as the best separated model for the majority of the loss functions used (see Table 4).

The obtained results show that:

- The best growth function g (in the total porosity model) is the estimated constant function.
- Quadratic loss function results for the separated porosity models indicate g-linear as the best growth function.
- All loss functions point h_3 and h_1 as almost equally good nucleation material function. We suggest to select h_1 because it is easier to interpret its parameters from the mechanical point of view.
- The total porosity model usually fits better the data.

We would like to stress that our material function was determined with the following important assumptions. The matrix material is plastically incompressible ($\dot{\rho}_m = 0$ where ρ_m is matrix density) and the elastic part of a strain-rate

tensor is neglected, $D_{ij} = D^p_{ij}$. All our conclusions concern exclusively the ductile steel material; although qualitative conclusions may be valid also for other types of materials.

Acknowledgments

The work of Z.N. has been prepared in partly within the framework of the research project of the Polish Committee for Scientific Research (KBN) Grant 7T11F 01921.

References

1. P.W. BRIDGMAN, *Studies in large plastic flow and fracture*, McGraw-Hill, 1952.
2. M. SAJE, J. PAN and A. NEEDLEMAN, *Void nucleation effects on shear localization in porous plastic solids*, Int. J. Fracture, **19**, 163, 1982.
3. J. CHAKRABARTY, *Applied plasticity*, Springer-Verlag, New York, 2000.
4. A.L. GURSON, *Continuum theory of ductile rupture by void nucleation and growth. Part 1. Yield criteria and flow rules for porous ductile media*, J. Engng. Materials and Technology, Trans. of the ASME, **99**, 2–15, 1977.
5. K.A. CLARKE, *Testing nonnested models of international relations: reevaluating realism*, American Journal of Political Science, **45**, 1–62, 2001.
6. M. MCALEER, *The significance of testing empirical non-nested models*, Journal of Econometrics, **67**, 149–171, 1995.
7. J.R. FISHER, *Void nucleation in spheroidized steels during tensile deformation*, Ph.D. Thesis, Brown University, 1980.
8. J. R. FISHER and J. GURLAND J, *Void nucleation in spheroidized carbon steels. Part 1: Experimental*, Metal Science, **15**, 5, 185–192, 1981.
9. P.J. HUBER, *Robust methods of estimation of regression coefficients*, Math. Operationsforsch. Stat., Ser., Stat., **8**, 141–153, 1977.
10. M. GOLOGANU, J.-B. LEBLOND, G. PERRIN and J. DEVAUX, *Recent extensions of Gurson's model for porous ductile metals*, [in:] Continuum micromechanics P. SUQUET [Ed.], 61–130, Springer, Berlin 1995.
11. A.L. GURSON, *Continuum theory of ductile rupture by void nucleation and growth. Part 1. Yield criteria and flow rules for porous ductile media*, J. Engng. Materials and Technology, Trans. of the ASME, **99**, 2–15, 1977.
12. J. GURLAND, *Observations on the fracture of cementite particles in spheroidized 1.05%C steel deformed at room temperature*, Acta Metall., **20**, 735–741, 1972.
13. J. KOPLIK and A. NEEDLEMAN, *Void growth and coalescence in porous plastic solids*, Int. J. Solids Structure, **24**, 835–853, 1988.
14. J.-B. LEBLOND, G. PERRIN and J. DEVAUX, *An improved Gurson-type model for hardenable ductile metals*, European Journal of Mechanics A/Solids, **14**, 499–527, 1995.

15. G.C. LI X.W. LING and H. SHEN *On the mechanism of void growth and the effect of straining mode in ductile materials*, Int. J. Plasticity, **16**, 39–58, 2001.

16. F.A. MCCLINTOCK, *A criterion for ductile enlargement of voids in triaxial stress fields*, ASME Journal of Applied Mechanics, **4**, 363—71, 1968.

17. B. BUDIANSKY, JW. HUTCHINSON, S. SLUTSKY *Void growth and collapse in viscous solids*, [in:] HG. HOPKINS, M.J. SEWELL [Eds.], Mechanics of solids, Oxford, Pergamon, 1344, 1982.

18. J.R. RICE, D.M. TRACEY, *On the ductile enlargement of voids in triaxial stress fields*, J. Mech. Phys. Solids, **17**, 201–217, 1969.

19. GOTOH MANABU, YAMASHITA MINORU, *An aspect of plasticity with compressibility*, Int. Journal of Plasticity, **19**, 383—401, 2003.

20. A.A. BENZERGA, *Micromechanics of coalescence in ductile fracture*, J. Mech. Phys. Solids, **50**, 1331–1362, 2002.

21. F.M. BEREMIN, *Experimental and numerical study of the different stages in ductile rupture: application to crack initiation and stable crack growth*, [in:] S. NEMAT-NASSER, [Ed.], Three-Dimensional Constitutive relations of Damage and Fracture, Pergamon Press, 157—172, New York 1981.

22. M. GOLOGANU, J.-B. LEBLOND, J. DEVAUX, *Approximate models for ductile metals containing non-spherical voids — case of axisymmetric prolate ellipsoidal cavities*, J. Mech. Phys. Solids, **41**, 11, 1723-–1754, 1993.

23. M. GOLOGANU, J.-B. LEBLOND, J. DEVAUX, *Numerical and theoretical study of coalescence of cavities in periodically voided solids*, [in:] A. NEEDLEMAN [Ed.], Computational Material Modeling, ASME, 223-–244, New York 1994.

24. M. GOLOGANU, J.-B. LEBLOND, G. PERRIN, J. DEVAUX, *Recent extensions of Gurson's model for porous ductile metals*, [in:] P. SUQUET, [Ed.], Continuum micromechanics, Springer, 61—130, Berlin 1995.

25. M. GOLOGANU, J.-B. LEBLOND, G. PERRIN, J. DEVAUX, *Theoretical models for void coalescence in porous ductile solids — I: coalescence in "layers"*, Int. J. Solids Struct., **38**, 32—33, 5581–5594, 2001.

26. M. GARAJEU, J.C. MICHEL, P. SUQUET, *A micromechanical approach of damage in viscoplastic materials by evolution in size, shape and distribution of voids*, Comput. Methods Appl. Mech. Eng., 183, 223—246, 2000.

27. A. NEEDLEMAN, J.R. RICE *Limits to ductility set by plastic flow localization*, [in:] Mechanics of Sheet Metal Forming, 237–267, [Eds.] D.P. KOISTINEN and N.-M. WANG, Plenum, New York 1978.

28. Z. NOWAK, A. STACHURSKI, *Nonlinear regression problem of material functions identification for porous media plastic flow*, *Engineering Transactions*, **49**, 637–661, 2001.

29. Z. NOWAK, A. STACHURSKI, *Global optimization in material functions identification for voided plastic flow*, Computer Assisted Mech. and Engng. Sciences, **9**, 205–221, 2002.

30. Z. NOWAK, A. STACHURSKI, *Modelling and identification of voids nucleation and growth effects in porous media plastic flow*, Control and Cybernetics, **32**, 819–849, 2003.

31. M. GOTOH and M. YAMASHITA, *An aspect of plasticity with compressibility* Int. J. of Plasticity, **19**, 383–401, 2003.

32. T. PARDOEN and F. DELANNAY, *Assessment of void growth models from porosity measurements in cold-drawn copper bars* Metallurgical and Materials Transactions, **29A**, 1895–1909, 1998.

33. T. PARDOEN, I. DOGHRI and F. DELANNAY, *Experimental and numerical comparison of void growth models and void coalescence criteria for the prediction of ductile fracture in copper bars*, Acta Materialia, **46**, 541–552, 1998.

34. T. PARDOEN and J.W. HUTCHINSON, *An extended model for void growth and coalescence*, Journal Mech. Phys. Solids, **48**, 2467–2512, 2000.

35. B. MARINI, F. MUDRY and A. PINEAU, *Experimental study of cavity growth in ductile rupture*, Engng Fracture Mechanics, **6**, 989–996, 1985.

36. P. PERZYNA, *Constitutive modelling of dissipative solids for postcritical behaviour and fracture*, ASME J. Eng. Materials and Technology, **106**, 410–419, 1984.

37. P. PERZYNA and Z. NOWAK, *Evolution equation for the void fraction parameter in necking region*, Arch. Mech., **39**, 1–2, 73–84, 1987.

38. G.A.F. SEBER, C.J. WILD, *Nonlinear Regression*, John Wiley and Sons, NY 1989.

39. O.P. SØVIK and C. THAULOW, *Growth of spherical void in elastic-plastic solids*, Fatigue Fract. Engng Mater. Struct., **20**, 12, 1731–1744, 1997.

40. C.C. CHU, A. NEEDLEMAN, *Void nucleation effects in biaxially stretched sheets*, Trans. ASME, J. Engng., Materials and Technology, **102**, 249–256, July 1980.

41. V. TVERGAARD, *Material failure by void growth to coalescence*, Adv. Appl. Mech., **27**, 83–151, 1990.

42. SÖDERSTRÖM T. and STOICA P., *System Identification*, Prentice Hall, International University Press, Cambridge,1989.

43. C.G. BOENDER, A.H.G. RINNOOY KAN, L. STROUGIE and G.T. TIMMER *A Stochastic Method for Global Optimization*, Mathematical Programming, **22**, 125–140, 1982.

44. A. TÖRN and A. ŽILINSKAS, *Global Optimization*, Springer Verlag, Berlin, Heidelberg, 1989.

45. W.H. PRESS, S.A. TEUKOLSKY, W.T. VETTERLING and B.P. FLANNERY, *Numerical Recipes in C: The Art of Scientific Computing*, Cambridge University Press, Cambridge, 1993.

46. Q. VUONG, *Likelihood ratio tests for model selection and nonnested hypothesis*, *Econometrica*, **57**, 307–333, 1989.

Received September 23, 2005; revised version January 25, 2006.